Porphyrinic Metal–Organic Framework PCN-224 Nanoparticles for Near-Infrared-Induced Attenuation of Aggregation and Neurotoxicity of Alzheimer's Amyloid-β Peptide

Jiuhai Wang, Yadi Fan, Youhua Tan, Xin Zhao, Yu Zhang, Changming Cheng*, and Mo Yang*

Abstract

The aberrant aggregation of amyloid-β peptide (Aβ) in the brain has been considered as the major pathological hallmark of Alzheimer's diseases (AD). Inhibition of Aβ aggregation is considered as an attractive therapeutic intervention for alleviating amyloid-associated neurotoxicity. Here, we report the near-infrared light (NIR)-induced suppression of Aβ aggregation and reduction of Aβ-induced cytotoxicity via porphyrinic metal–organic framework (MOF) PCN-224 nanoparticles. PCN-224 nanoparticles are hydrothermally synthesized by coordinating tetra-kis(4-carboxyphenyl)porphyrin (TCPP) ligands with zirconium. The PCN-224 nanoparticles show high photo-oxygenation efficiency, good biocompatibility, and high stability. The study reveals that the porphyrinic MOF-based nanoprobe activated by NIR light could successfully inhibit self-assembly of monomeric Aβ into a β-sheet-rich structure. Furthermore, photoexcited PCN-224 nanoparticles also significantly reduce Aβ-induced cytotoxicity under NIR irradiation.

KEYWORDS: metal−organic framework Alzheimer's disease phototherapy PCN-224 amyloid-β

Alzheimer's disease (AD) is a progressive, unremitting neurodegenerative disorder that presents mostly in the elderly population with a progressive impairment of the patient's cognitive and memory ability. (1) Although the exact biological mechanism behind this disease is not clearly elucidated yet, it is believed that AD is associated with the abnormal accumulation of soluble monomers of amyloid-β 1–42 (Aβ42) peptide into extracellular oligomers and fibrillary deposits with β-sheet-rich structures. (2,3) The elevated production and impaired clearance of oligomeric and fibrillary Aβ42 peptide in the brain of AD patients is highly correlated with the onset of neurotoxicity. (4,5)

The suppression of Aβ aggregation is considered to be an attractive approach for treating AD disease. Recent studies revealed that transformation of native Aβ to oxygenated forms via photooxygenation could successfully suppress Aβ aggregation and neurotoxicity. (6,7) Generally, oxygenated Aβ monomer has poor aggregation capability compared to native Aβ monomer. Various photosensitizers have been used for light-induced suppression of Aβ42 aggregation. (8−10) However, these organic photosensitizers suffer from poor water dispersity and low photostability. Moreover, the delivery of light into the brain tissue through the skull has always been a challenge for light-based therapy in neuroscience fields. Most of the above photosensitizers for suppression of Aβ aggregation were still in the visible-light range with limited penetration depth.

More recently, nanoparticle-based photooxygenation strategy has been explored for suppression of

Aβ aggregation. Chung et al. used carbon nanodot and graphitic carbon nitride nanosheets (g-C3N4) as a photosensitizers to inhibit the aggregation of Aβ42 peptide, which showed good water dispersity and photostability in the visible-light window. (11,12) Kuk et al. developed a hybrid nanoplatform composed of Yb/Er-co-doped NaYF4 up-conversion nanoparticles (UCNP) and organic photosensitizer rose bengal (RB) for near-infrared (NIR)-light-induced suppression of Aβ aggregation. (13) In this hybrid system, UCNP was used as an energy transducer to transfer NIR light to visible light for the activation of organic photosensitizer. However, the generally low quantum yield (<1%) of UCNPs, (14) and the two-stage photoactivation process may result in a low efficiency of photo-oxygenation. Therefore, the development of NIR-light induced inhibition of Aβ aggregation based on new nanomaterials with high photo-oxygenation efficiency and high stability is of high importance.

Metal–organic framework (MOF) is an emerging hybrid nanomaterial family that has attracted growing interest due to its porous structure, good biocompatibility, and tunable size. (15−19) In this letter, we report NIR-light-induced efficient inhibition of Alzheimer's amyloid-β peptide aggregation based on porphyrinic Zr metal–organic framework (MOF) PCN-224 nanoparticles (Scheme 1). The synthesized PCN-224 nanoparticles with the integration of tetra-kis(4-carboxyphenyl)porphyrin (TCPP) as ligands into the porous structure of MOF showed high singlet-oxygen generation capability in NIR window, good biocompatibility, and excellent stability in physiological environment. This porphyrinic MOF-based nanoprobe activated by NIR light could efficiently inhibit self-assembly of monomeric Aβ into β-sheet-rich structure. Furthermore, photoexcited PCN-224 nanoparticles also significantly reduced Aβ-induced cytotoxicity under NIR irradiation.

Scheme 1

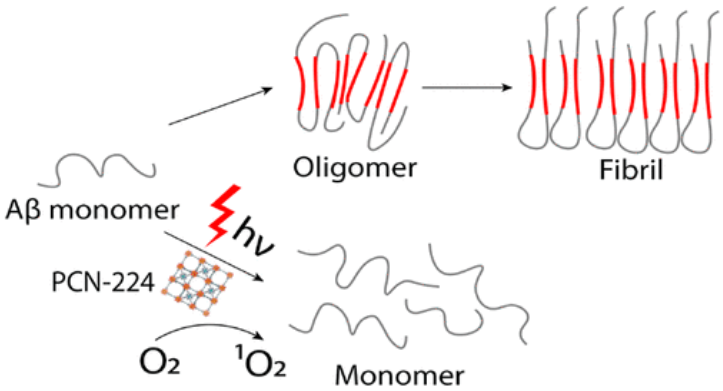

Scheme 1. Schematic Diagram of the Photo-inhibition of $A\beta_{42}$ Aggregation by PCN-224 Nanoparticles

PCN-224 nanoparticles were first synthesized in a diluted material system and then were characterized with various methods. PCN-224 has a stable crystalline framework structure consisting of Zr4+ and ligands, where metal atoms and ligands are coordinated through covalent bonding (Figure 1a). Zr is known for its good biocompatibility and high valence to link with bridging ligands to form an ultrastable Zr MOF structure. (20,21) When photosensitizer molecule TCPP is used as the ligand to build PCN-224, the generated porphyrinic MOF structure would have high light-to-oxygen generation due to the high density of TCPP ligands in the framework and easy diffusion of molecular oxygen through the porous structure. (22,23) Moreover, the nanosized MOF

structures are preferred for potential brain delivery to across the blood–brain barrier (BBB). It has been demonstrated that nanoparticles with small size within 10–100 nm could promote the BBB permeability. (24) However, downsizing MOF to the nanoscale is always challenging because it is easy to form undesired phases during crystallization. (25) Here, Zr-based MOF PCN-224 was hydrothermally synthesized in a diluted system aiming at creating more MOF monomers, which would result in smaller nanoparticles. Transmission electronic microscopy (TEM) image showed that the synthesized PCN-224 nanoparticles had round-shape (Figure 1b). Field-emission scanning electron microscopy (FESEM) images were also taken to analyze the size distribution of PCN-224 nanoparticles (Figure S1), which showed an average size around 70 nm (Figure 1c). Dynamic light scattering (DLS) was also used to measure the size of PCN-224 nanoparticles in water, which matched well with the results from SEM analysis (Figure S2). The UV–visible absorption spectra of PCN-224 nanoparticles showed a main absorption peak at 425 nm (Figure 1d) and four other peaks between 500 and 700 nm (see the inset of Figure 1d). The four small peaks were attributed to the Q bands of porphyrin ligands inside nanoparticles between 500 and 700 nm. (26) The absorption peak at 650 nm of PCN-224 nanoparticle indicated the possibility of NIR activated photo-oxygenation. The photoluminescence (PL) spectra of PCN-224 nanoparticles showed an emission peak at 680 nm under an excitation wavelength of 440 nm, which demonstrated the possibility to use red fluorescence as cell imaging labels (Figure 1e). The fluorescence quantum yield of PCN-224 nanoparticles was measured to be 17% at 25 °C, which is much higher than the common quantum yield of up-conversion nanoparticles around 1%.

Figure 1

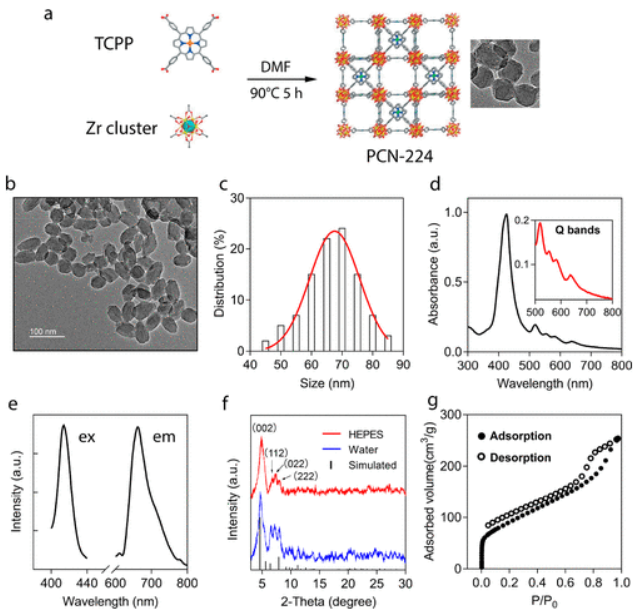

Figure 1. Characterizations of PCN-224 nanoparticles. (a) Schematic illustration of the synthesis of PCN-224 nanoparticles. (b) TEM image of PCN-224 nanoparticles. (c) Size distribution of PCN-224 nanoparticles by TEM. (d) UV-vis absorbance spectra of PCN-224 nanoparticles (inset figure: the enlarged region of 500−800 nm). (e) Excitation and emission spectra of PCN-224 nanoparticle. PCN-224 nanoparticle has a highest excitation wavelength at 414 nm (left curve) and an emission peak at wavelength of 650 nm. (f) Powder XRD of PCN-224 nanoparticles. (g) N_2 adsorption−desorption isotherms of the PCN-224 nanoparticles.

PCN-224 nanoparticles were further characterized by ζ potential measurement, powder X-ray diffraction (PXRD), thermogravimetric analysis (TGA), Fourier transform infrared spectroscopy (FTIR) and Brunauer–Emmett–Teller (BET) analysis. PCN-224 nanoparticles showed good

dispersibility in water and HEPES buffer after 7 days standing by comparison with the solutions on the first day (Figure S3). The ζ potential of PCN-224 nanoparticle was around +25.8 mV in water and −24.5 mV in HEPES buffer at pH 7, which explained its good dispersibility in water and HEPES buffer (Figure S4). The PXRD was used to further determine the crystallinity of PCN-224 nanoparticles. The PXRD pattern of as-synthesized PCN-224 registered with 2θ steps of 0.02° agreed well with the simulated curve in Figure 1f. The different peaks at 4.591°, 5.623°, 6.494°, and 7.956° represent the crystal plane [002], [112], [022], and [222], respectively. Notably, PXRD curve of PCN-224 nanoparticle maintained unchanged in HEPES buffer (20 μM, pH 7.4) compared with those in water, indicating that PCN-224 retained good stability in HEPES buffer for 24 h. The as-prepared PCN-224 was also analyzed by thermogravimetric analysis (TGA) (Figure S5). The first step of weight loss of 23% in the region of 50–240 °C was due to the removal of adsorbed water and organic solvent inside the PCN-224 pores. The second step of weight loss occurred between 400 and 580 °C, which was attributed to the loss of organic ligands. The FTIR spectra in Figure S6 indicated the presence of O–H bond at around 1440 cm–1. The peaks between 1620 and 1690 cm–1 were attributed to the C=O stretching due to the coordination with metal ions and the peak at 650 cm–1 is owing to Zr–OH bond. The surface area of PCN-224 nanoparticles was determined by N2 adsorption using a dynamic Brunauer–Emmett–Teller (BET) method. The BET surface area was measured to be 326.34 m2g–1, showing the porosity of the PCN-224 nanoparticles (Figure 1g). PCN-224 exhibited excellent photostability under laser illumination at 650 nm with a power density of 0.5 W/cm2 for 30 min, where no obvious change could be observed in UV–vis absorption spectra (Figure S7).

We further investigated the photoinduced inhibitory effect of PCN-224 nanoparticles on the aggregation of Aβ42 peptide under a CEL-500 xenon lamp with a 650 nm filter. Aβ42 peptide was treated with PCN-224 nanoparticles under light irradiation at 650 nm for 30 min (30 mW/cm2) and then incubated at 37 °C up to 96 h. Thioflavin T (ThT) assay was used to monitor the aggregation degree of Aβ42 peptide. ThT is a probe dye that specifically binds to the β-sheet-rich amyloid peptide with a significant fluorescence increase at the wavelength of 485 nm. As shown in Figure 2a, the ThT fluorescence intensities increased to maximum after 24 h incubation in all conditions. The steady increase of ThT fluorescence intensity at 485 nm in dark environment without nanoparticles indicated the self-assembly aggregation of monomeric Aβ42 peptide (Figures 2a and S8). In the presence of PCN-224 nanoparticles alone or light irradiation alone, the ThT fluorescence intensity versus time curves are almost identical to that obtained in the dark environment, which indicated that light irradiation on Aβ42 alone or incubation with nanoparticles alone could not affect the aggregation of Aβ42 peptide (Figure 2a). ThT fluorescence intensity did not differ significantly after 96 h of incubation among the three cases with only nanoparticles, only light, and no nanoparticles in the dark environment (Figure 2b). However, when monomeric Aβ42 peptide solution was treated with PCN-224 nanoparticles under 650 nm light illumination, ThT fluorescence intensity remained low (Figure 2a,b). This indicated that photoactivated PCN-224 nanoparticles could effectively inhibit the aggregation of Aβ42 into a high-order β-sheet-rich structure. Moreover, a concentration-dependent photoinhibition by PCN-224 nanoparticles was observed (Figure 2c). Generally, Aβ aggregation degree was gradually decreased with the increasing concentrations of PCN-224 nanoparticles. When the concentration of PCN-224 nanoparticles reached 100 μg/mL, the further increase of particle concentration did not significantly reduce Aβ aggregation.

Figure 2

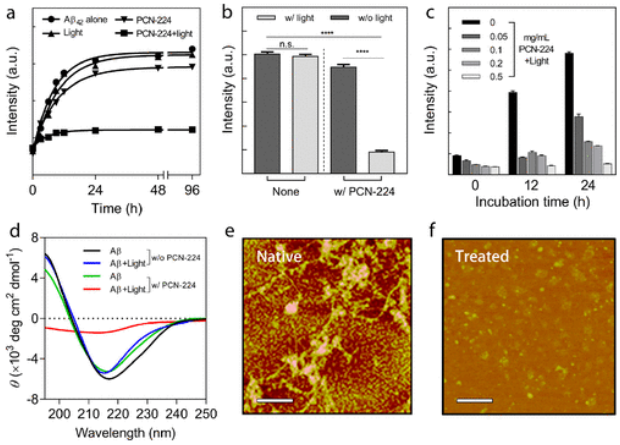

Figure 2. Photoinhibitory effect of PCN-224 nanoparticles on the $A\beta_{42}$ aggregation. $A\beta_{42}$ peptide was treated with PCN-224 nanoparticles under light irradiation at 650 nm for 30 min (30 mW/cm^2) and then incubated at 37 °C from 24 to 96 h. (a) ThT fluorescence intensity vs time curves of $A\beta_{42}$ incubated in the dark environment without nanoparticles in the presence of PCN-224 nanoparticle alone, in the presence of light irradiation alone, and in the presence of PCN-224 nanoparticles under light irradiation up to 96 h. (b) ThT fluorescence intensities of $A\beta_{42}$ after incubation of 24 h with different treatments. One-way analysis of variance was used for data analysis (quadruple asterisks indicate $p < 0.0001$, and n.s. is not significant). (c) ThT fluorescence intensities of $A\beta_{42}$ treated with different amount of PCN-224 nanoparticles under light irradiation and then incubated at 37 °C for 0, 12, and 24 h, respectively. (d) CD spectra of $A\beta_{42}$ peptide (25 μM) with different treatments. (e) AFM image of the self-assembly of native $A\beta_{42}$. (f) AFM image of $A\beta_{42}$ peptide treated with 0.5 mg/mL of PCN-224 nanoparticles and light irradiation for 30 min. Scale bars indicate 500 nm. Both samples were incubated at 37 °C for 24 h before AFM measurements.

Considering that illumination is essential and necessary for PCN-224 nanoparticles to suppress Aβ42 self-assembly, we evaluated the effect of illumination time and power density of light on Aβ42 aggregation inhibition. Not surprisingly, ThT fluorescence intensity at 485 nm was reduced accordingly with the increase of illumination time and power density of light (Figures S9 and S10). Circular dichroism (CD) was further employed to confirm the photoinhibitory effect of PCN-224 nanoparticles on Aβ42 aggregation. As shown in Figure 2d, CD spectra of Aβ42 incubated without PCN-224 nanoparticles under dark environment exhibited a characteristic positive peak and a characteristic negative peak at 195 and 215 nm, respectively. This indicated the transition of Aβ secondary structure from random coil to β-sheet-rich structure. With PCN-224 nanoparticle alone or light irradiation alone, there was negligible change of CD spectra. However, the characteristic CD peaks completely disappeared in the presence of PCN-224 nanoparticles under 650 nm light illumination. The results here demonstrated that photoactivated PCN-224 nanoparticles could efficiently inhibit Aβ42 inhibition. In addition, atomic force microscopy (AFM) was also employed to analyze the aggregation degree of Aβ42 peptide. Figure 2e showed the formation of dense networks of Aβ fibrils after 24 h incubation of Aβ42 peptide without PCN-224 nanoparticles under dark environment. In the presence of PCN-224 nanoparticles under 650 nm light illumination, no obvious formation of Aβ fibrils was observed (Figure 2f).

The effect of photoactivated PCN-224 nanoparticles on the attenuation of Aβ aggregation was further studied with TEM, native gel electrophoresis, and dynamic light scattering (DLS). Aβ42 peptide was treated with PCN-224 nanoparticles of 100 μg/mL under light irradiation at 650 nm (30 mW/cm2) for 30 min following by incubation at 37 °C up to 24 h. As evidenced by TEM, highly aggregated fibrils were observed for Aβ42 incubated without PCN-224 nanoparticles under a dark

environment (Figure 3a). In contrast, photoactivated PCN-224 nanoparticle treated Aβ42 did not transform to fibrils after 24 h of incubation (Figure 3b). Native gel electrophoresis was utilized to measure the molecular weight change of Aβ42 peptide under various treatments (Figure 3c). It was observed that large oligomers and fibrils (∼90–170 kDa) were formed in Aβ42 without incubation with PCN-224 nanoparticles in the dark environment (lane 1), Aβ42 with light irradiation alone (lane 2), and Aβ42 with PCN-224 nanoparticles alone (lane 3). In the presence of PCN-224 nanoparticles with light irradiation (lane 4), a monomeric band (∼4.5 kDa) and a dimeric band (∼9 kDa) were observed, which demonstrated the inhibition effect of photoactivated PCN-224 nanoparticles. PCN-224 nanoparticle alone did not show any bands in lane 5 due to its positive charge, demonstrating that the nanoparticles did not interfere with the native gel electrophoresis results. DLS analysis was used to further determine the size dynamic change of the Aβ42 peptide before and after the treatment by photoactivated PCN-224 nanoparticles (Figure 3d). PCN-224 nanoparticles were removed by centrifugation before the DLS analysis. Obviously, Aβ42 incubated without PCN-224 nanoparticles under dark environment showed a gradually increased size from around 50 nm to around 700 nm after 24 h incubation due to the formation of Aβ fibrils. In contrast, Aβ42 treated with photoactivated PCN-224 nanoparticles under light irradiation remained as structures under 100 nm after 24 h incubation.

Figure 3

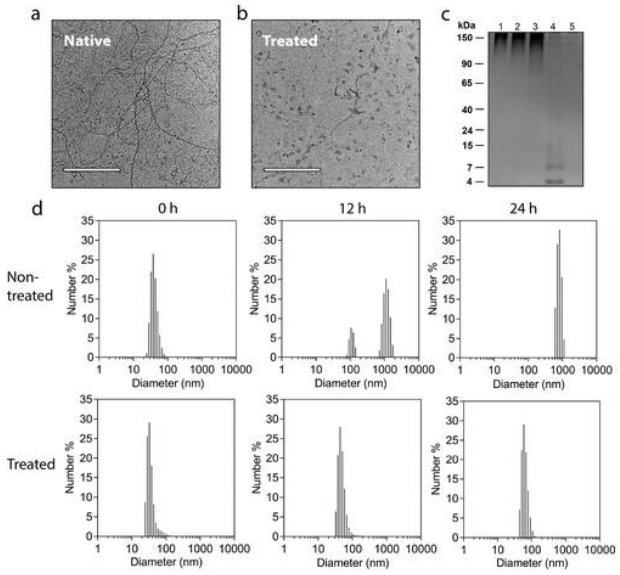

Figure 3. (a) TEM image of nontreated $A\beta_{42}$ incubated at 37 °C for 24 h. (b) TEM image of $A\beta_{42}$ treated with PCN-224 nanoparticles with a concentration of 100 μg/mL under light irradiation at 650 nm (30 mW/cm^2) for 30 min following by incubation for 24 h at 37 °C. Scale bars indicate 0.5 μm. (c) Native gel electrophoresis of $A\beta_{42}$ with different treatments. Lane 1: $A\beta_{42}$ without PCN-224 nanoparticle in the dark environment; Lane 2: $A\beta_{42}$ with light irradiation alone; Lane 3: $A\beta_{42}$ with PCN-224 nanoparticles alone; Lane 4: $A\beta_{42}$ with PCN-224 nanoparticles under light irradiation; Lane 5: PCN-224 nanoparticles alone. (d) DLS size distribution of monomeric $A\beta_{42}$ without treatment and treated with PCN-224 nanoparticles under light irradiation over 24 h of incubation at 37 °C.

The light-induced inhibition on Aβ42 inhibition could attribute to the generation of reactive oxygen species (ROS) by photoactivated PCN-224 nanoparticles. According to the literature, porphyrinic MOFs have been reported to be effective photosensitizers for singlet oxygen (1O2) generation. (21,22) We measured the capability of the 1O2 generation of PCN-224 nanoparticles with a concentration of 100 μg/mL under 650 nm light illumination. 1,3-Diphenylisobenzofuran (DPBF), a sensitive 1O2-trapping reagent, was used to explore 1O2 generation capabilities of PCN-224

nanoparticles based on absorbance peak at 414 nm. The remarkable reduction of DPBF absorbance at 414 nm with the increase of irradiation time indicated the high 1O2 production capability of PCN-224 nanoparticles (Figure 4a). Using the common photosensitizer rose bengal (RB) as the reference, PCN-224 nanoparticles showed a higher 1O2 production capability under the same conditions in the DPBF absorbance versus time curves (Figure 4b). The production of 1O2 by PCN-224 nanoparticles was further demonstrated by 2′,7′-dichlorodihydrofluorescein diacetate (DCFH-DA) fluorescence assay and electron spin resonance (ESR) under light illumination. As shown in Figure S11, the fluorescence intensity of DCFH-DA at wavelength of 541 nm increased significantly in the presence of PCN-224 under 650 nm light irradiation, which was due to the oxidization of nonfluorescent 2′,7′-Dichlorofluorescin diacetate and transformation to highly fluorescent 2′,7′-Dichlorofluorescein. As shown in Figure S12, ESR signal intensity significantly increased upon light illumination, which demonstrated the generation of 1O2 by photoexcited PCN-224 nanoparticles. The oxidation of Aβ42 by singlet oxygen was then verified by a 2,4-dinitrophenylhydrazine (DNPH) assay. Generally, protein oxidation by ROS could generate carbonyl group on protein side chains. (27) The DNPH assay is a sensitive assay for reaction with the carbonyl group on oxidized protein and results in the formation of a stable 2,4-dinitrophenyl (DNP) hydrazone product with a characteristic absorption peak at 370 nm. (23) As shown in Figure 4c, only Aβ42 treated with PCN-224 nanoparticles under light irradiation showed increased amplitude for absorption peak at 370 nm, which indicated the oxidation of Aβ42.

Figure 4

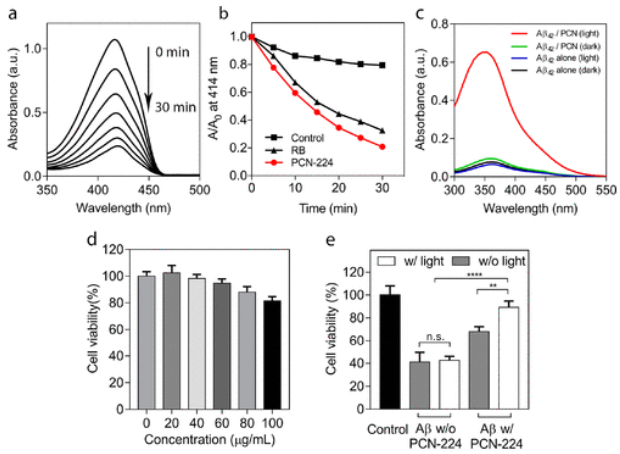

Figure 4. Photo-oxygenation capability tests for PCN-224 nanoparticles. (a) UV−vis spectra of DPBF assay was used as singlet oxygen indicator to evaluate the ROS generation ability of PCN-224 nanoparticles with a concentration of 100 μg/mL. (b) Absorbance of DPBF at 414 nm decreased significantly compared to the control group (in the absence of PCN-224). PCN-224 nanoparticles showed even higher photo-oxygenation capability compared to the classic photosensitizer rose bengal in the same condition. (c) DNPH assay of $A\beta_{42}$ with different treatments to show the protein oxidation degree. (d) Cytotoxicity of PCN-224 nanoparticles. (e) PC12 cell viability treated under various conditions. One-way analysis of variance was used for data analysis (double asterisks indicate $p < 0.01$, quadruple asterisks indicate $p < 0.0001$, and n.s. is not significant).

Next, we investigated the ability of photoactivated PCN-224 nanoparticles to reduce Aβ-induced cytotoxicity in PC12 cells using a 3-(4,5-dimethylthiazol-2yl)-2,5-diphenyltetrazolium bromide (MTT) assay. The PCN-224 nanoparticle itself showed good biocompatibility with a high cell viability over 80%, even at high concentrations up to 100 μg/mL (Figure 4d). The high cytotoxicity of Aβ42 aggregates assembled under dark environment or with light irradiation was observed with a low cell viability around 40% after 24 h incubation (Figure 4e). In contrast, cell viability was

largely increased to 90% when Aβ42 was incubated with PCN-224 nanoparticles under 650 nm light irradiation. The cell viability was around 65% with Aβ42 incubated with PCN-224 nanoparticles alone under dark environment. This increase of cell viability could be attributed to the physical absorption of Aβ42 onto PCN-224 nanoparticles, which led to a slightly low toxicity to cells. Adhesion of Aβ to the surface of the PCN-224 nanoparticles could reduce the active sites in the peptide for aggregation. Moreover, adhesion of Aβ to the surface PCN-224 nanoparticles could also increase the efficiency of local photo-oxidation treatment because the generated singlet oxygen molecules could rapidly dissipate from the surface of the nanoparticles. Overall, the nanoparticle-based light-induced photo-oxygenation process have a synergistic effect on the suppression of Aβ-induced cytotoxicity by inhibiting aggregation of monomeric Aβ42 peptide.

In conclusion, we have developed a facile strategy for NIR-light-induced inhibition of cross-β-sheet aggregation of Aβ42 peptide using photoactivated PCN-224 nanoparticles. Inspired by the photooxygenation ability of porphyrinic TCPP ligand in NIR region, we successfully synthesized PCN-224 MOF nanoparticles for NIR-light-induced inhibition of Aβ42 aggregation. We found that photoactivated PCN-224 nanoparticles were able to attenuate the aggregative activity of Aβ42 as well as decrease cytotoxicity for PC12 cells. The current approaches to suppress Aβ aggregation are mainly based on anti-Aβ targeting molecules capable of suppressing Aβ aggregation and neurotoxicity. (28,29) However, a majority of the above organic inhibitors show moderate inhibition capabilities for suppressing Aβ aggregation and suffer from rapid degradation in plasma. Photo-oxygenation approach is a promising approach to suppress Aβ aggregation with high inhibition efficiency. However, the usage of organic photosensitizers for photo-oxygenation leads to low water solubility, visible light excitation with limited penetration depth and poor stability in physiological environment. Compared with the above approaches, this NIR-light-induced photooxygenation approach based on PCN-224 nanoparticles could provide four main advantages: (1) water dispersity and photostability in the physiological environment are good; (2) porphyrinic MOF nanoparticles could deliver NIR light to the deep brain more efficiently compared to visible light used in other studies; (3) functional porphyrinic linkers are spatially separated by Zr cluster in MOF framework, which provides high single-oxygen-generation capability by avoiding self-quenching of the excited state and keeping the photooxygenation property of each porphyrinic linker; (4) porous MOF structure facilitates the easy diffusion of molecular oxygen with the quick treatment of Aβ42 peptide. Overall, such NIR-light-triggered therapeutic photooxygenation of Aβ42 based on porphyrinic MOF nanoparticles is expected to hold great promise for the non-invasive phototreatment of neurodegenerative diseases.

Acknowledgments

This work was supported by the National Natural Science Foundation of China (NSFC) (grant no. 81471747 and 31771077) and The Hong Kong Polytechnic University Internal Fund (grant nos. 1-ZVJ7 and 1-YW1L). This work was also supported by the University Research Facility in Life Sciences of the Hong Kong Polytechnic University.

(1) Scheltens, P.; Blennow, K.; Breteler, M. M. B.; de Strooper, B.; Frisoni, G. B.; Salloway, S.; Van der Flier, W. M. Alzheimer's Disease. Lancet 2016, 388, 505−517.

(2) Haass, C.; Selkoe, D. J. Soluble Protein Oligomers in Neurodegeneration: Lessons from the

Alzheimer's Amyloid Beta Peptide. Nat. Rev. Mol. Cell Biol. 2007, 8, 101−112.
(3) Hardy, J.; Selkoe, D. J. The Amyloid Hypothesis of Alzheimer's Disease: Progress and Problems on the Road to Therapeutics. Science 2002, 297, 353.
(4) Benilova, I.; Karran, E.; De Strooper, B. The Toxic A Beta Oligomer and Alzheimer's Disease: An Emperor in Need of Clothes. Nat. Neurosci. 2012, 15, 349−357.
(5) Ghosh, A. K.; Brindisi, M.; Tang, J. Developing Ss-Secretase Inhibitors for Treatment of Alzheimer's Disease. J. Neurochem. 2012, 120, 71−83.
(6) Taniguchi, A.; Shimizu, Y.; Oisaki, K.; Sohma, Y.; Kanai, M. Switchable Photooxygenation Catalysts that Sense Higher-Order Amyloid Structures. Nat. Chem. 2016, 8, 974−982.
(7) Binger, K. J.; Griffin, M. D.; Howlett, G. J. Methionine Oxidation Inhibits Assembly and Promotes Disassembly of Apolipoprotein C-II Amyloid Fibrils. Biochemistry 2008, 47, 10208−10217.
(8) Taniguchi, A.; Sasaki, D.; Shiohara, A.; Iwatsubo, T.; Tomita, T.; Sohma, Y.; Kanai, M. Attenuation of the Aggregation and Neuro□toxicity of Amyloid-Beta Peptides by Catalytic Photooxygenation. Angew. Chem., Int. Ed. 2014, 53, 1382−1385.
(9) Lee, J. S.; Lee, B. I.; Park, C. B. Photo-induced Inhibition of Alzheimer's Beta-Amyloid Aggregation In Vitro by Rose Bengal. Biomaterials 2015, 38, 43−49.
(10) Lee, B. I.; Suh, Y. S.; Chung, Y. J.; Yu, K.; Park, C. B. Shedding Light on Alzheimer's beta-Amyloidosis: Photosensitized Methylene Blue Inhibits Self-Assembly of beta-Amyloid Peptides and Disinte grates Their Aggregates. Sci. Rep. 2017, 7, 7523.
(11) Chung, Y. J.; Kim, K.; Lee, B. I.; Park, C. B. Carbon Nanodot Sensitized Modulation of Alzheimer's beta-Amyloid Self-Assembly, Disassembly, and Toxicity. Small 2017, 13, 1700983.
(12) Chung, Y. J.; Lee, B. I.; Ko, J. W.; Park, C. B. Photoactive g C3N4 Nanosheets for Light-Induced Suppression of Alzheimer's Beta-Amyloid Aggregation and Toxicity. Adv. Healthcare Mater. 2016, 5, 1560−1565.
(13) Kuk, S.; Lee, B. I.; Lee, J. S.; Park, C. B. Rattle-Structured Upconversion Nanoparticles for Near-IR-Induced Suppression of Alzheimer's beta-Amyloid Aggregation. Small 2017, 13, 1603139.
(14) Bagheri, A.; Arandiyan, H.; Boyer, C.; Lim, M. Lanthanide□Doped Upconversion Nanoparticles: Emerging Intelligent Light□Activated Drug Delivery Systems. Adv. Sci. 2016, 3, 1500437.
(15) Ali, Z.; Wang, J. H.; Tang, Y. J.; Liu, B.; He, N. Y.; Li, Z. Y. Simultaneous Detection of Multiple Viruses Based on Chemilumi nescence and Magnetic Separation. Biomater. Sci. 2017, 5, 57−66.
(16) Wang, J. H.; Lu, P.; Yan, J. N.; Zhang, Y. F.; Huang, L. Y.; Ali, Z. S.; Liu, B.; Li, Z. Y.; He, N. Y. Rapid and Sensitive Detection of RNA Viruses Based on Reverse Transcription Loop-Mediated Isothermal Amplification, Magnetic Nanoparticles, and Chemilumi□nescence. J. Biomed. Nanotechnol. 2016, 12, 710−716.
(17) Wang, J.; Fan, Y.; Lee, H. W.; Yi, C.; Cheng, C.; Zhao, X.; Yang, M. Ultrasmall Metal-organic Framework Zn-MOF-74 Nano□dots: Size-controlled Synthesis and Application for Highly Selective Colorimetric Sensing of Iron (III) in Aqueous Solution. ACS Appl. Nano Mater. 2018, 1, 3747−3753.
(18) Wang, J. H.; Ali, Z. S.; Wang, N. Y.; Liang, W. B.; Liu, H. N.; Li, F.; Yang, H. W.; He, L.; Nie, L. B.; He, N. Y.; Li, Z. Y. Simultaneous Extraction of DNA and RNA from Escherichia coli BL 21 Based on Silica-Coated Magnetic Nanoparticles. Sci. China: Chem. 2015, 58, 1774−1778.
(19) Wang, B.; Lv, X.-L.; Feng, D.; Xie, L.-H.; Zhang, J.; Li, M.; Xie, Y.; Li, J.-R.; Zhou, H.-C.

Highly Stable Zr(IV)-Based Metal−Organic Frameworks for the Detection and Removal of Antibiotics and Organic Explosives in Water. J. Am. Chem. Soc. 2016, 138, 6204− 6216.
(20) Park, J.; Jiang, Q.; Feng, D.; Mao, L.; Zhou, H. C. Size□Controlled Synthesis of Porphyrinic Metal-Organic Framework and Functionalization for Targeted Photodynamic Therapy. J. Am. Chem. Soc. 2016, 138, 3518−3525.
(21) Lu, K.; He, C.; Lin, W. A Chlorin-Based Nanoscale Metal− Organic Framework for Photodynamic Therapy of Colon Cancers. J. Am. Chem. Soc. 2015, 137, 7600−7603.
(22) Feng, D.; Chung, W.-C.; Wei, Z.; Gu, Z.-Y.; Jiang, H.-L.; Chen, Y.-P.; Darensbourg, D. J.; Zhou, H.-C. Construction of Ultrastable Porphyrin Zr Metal−Organic Frameworks through Linker Elimi nation. J. Am. Chem. Soc. 2013, 135, 17105−17110.
(23) Chen, Y.-Z.; Wang, Z. U.; Wang, H.; Lu, J.; Yu, S.-H.; Jiang, H.- L. Singlet Oxygen-Engaged Selective Photo-Oxidation over Pt Nanocrystals/Porphyrinic MOF: The Roles of Photothermal Effect and Pt Electronic State. J. Am. Chem. Soc. 2017, 139, 2035−2044.
(24) Saraiva, C.; Praca, C.; Ferreira, R.; Santos, T.; Ferreira, L.; Bernardino, L. Nanoparticle-mediated Brain Drug Delivery: Over coming Blood−Brain Barrier to Treat Neurodegenerative Diseases. J. Controlled Release 2016, 235, 34−47.
(25) Diaz-Garcia, M.; Mayoral, A.; Diaz, I.; Sanchez-Sanchez, M. Nanoscaled M-MOF-74 Materials Prepared at Room Temperature. Cryst. Growth Des. 2014, 14, 2479−2487.
(26) Stradomska, A.; Knoester, J. Shape of The Q Band in The Absorption Spectra of Porphyrin Nanotubes: Vibronic Coupling or Exciton Effects? J. Chem. Phys. 2010, 133, 094701.
(27) Dalle-Donne, I.; Rossi, R.; Giustarini, D.; Milzani, A.; Colombo, R. Protein Carbonyl Groups as Biomarkers of Oxidative Stress. Clin. Chim. Acta 2003, 329, 23−38.
(28) Soto, C.; Sigurdsson, E. M.; Morelli, L.; Kumar, R. A.; Castano, E. M.; Frangione, B. Beta-Sheet Breaker Peptides Inhibit Fibrillo genesis in A Rat Brain Model of Amyloidosis: Implications for Alzheimer's Therapy. Nat. Med. 1998, 4, 822−826.
(29) McLaurin, J.; Kierstead, M. E.; Brown, M. E.; Hawkes, C. A.; Lambermon, M. H. L.; Phinney, A. L.; Darabie, A. A.; Cousins, J. E.; French, J. E.; Lan, M. F.; Chen, F. S.; Wong, S. S. N.; Mount, H. T. J.; Fraser, P. E.; Westaway, D.; St George-Hyslop, P. Cyclohexanehexol Inhibitors of Aβ Aggregation Prevent and Reverse Alzheimer Phenotype in A Mouse Model. Nat. Med. 2006, 12, 801−808.